

Pulse wave analysis with diffusing-wave spectroscopy

MARKUS BELAU, WOLFGANG SCHEFFER, AND GEORG MARET

Universität Konstanz, Fachbereich Physik, 78457 Konstanz, Germany

*markus.belau@uni-konstanz.de

Abstract: Hypertension is a major risk factor for cardiovascular disease and thus at the origin of many deaths by e.g. heart attack or stroke. Hypertension is caused by many factors including an increase in arterial stiffness which leads to changes in pulse wave velocity and wave reflections. Those often result in an increased left ventricular load which may result in heart failure as well as an increased pulsatile pressure in the microcirculation leading to damage to blood vessels. In order to specifically treat the different causes of hypertension it is desirable to perform a pulse wave analysis as a complement to measurements of systolic and diastolic pressure by brachial cuff sphygmomanometry. Here we show that Diffusing Wave Spectroscopy, a novel non-invasive portable tool, is able to monitor blood flow changes with a high temporal resolution. The measured pulse travel times give detailed information of the pulse wave blood flow profile.

References and links

1. S. Laurent, J. Cockcroft, L. Van Bortel, P. Boutouyrie, C. Giannattasio, D. Hayoz, B. Pannier, C. Vlachopoulos, I. Wilkinson, and H. Struijker-Boudier, "Expert consensus document on arterial stiffness: methodological issues and clinical applications," *European Heart Journal* **27**, 2588–2605 (2006).
2. R. R. Townsend, I. B. Wilkinson, E. L. Schiffrin, A. P. Avolio, J. A. Chirinos, J. R. Cockcroft, K. S. Heffernan, E. G. Lakatta, C. M. McEniery, G. F. Mitchell, S. S. Najjar, W. W. Nichols, E. M. Urbina, and T. Weber, "Recommendations for improving and standardizing vascular research on arterial stiffness a scientific statement from the American Heart Association," *Hypertension* **66**, 698–722 (2015).
3. I. Marshall, P. Papathanasopoulou, and K. Wartolowska, "Carotid flow rates and flow division at the bifurcation in healthy volunteers," *Physiological Measurement* **25**, 691–697 (2004).
4. M. D. Ford, N. Alperin, S. H. Lee, D. W. Holdsworth, and D. A. Steinman, "Characterization of volumetric flow rate waveforms in the normal internal carotid and vertebral arteries," *Physiological Measurement* **26**, 477–488 (2005).
5. M. N. Gwilliam, N. Hoggard, D. Capener, P. Singh, A. Marzo, P. K. Verma, and I. D. Wilkinson, "Mr derived volumetric flow rate waveforms at locations within the common carotid, internal carotid, and basilar arteries," *Journal of Cerebral Blood Flow and Metabolism* **29**, 1975–1982 (2009).
6. D. W. Holdsworth, C. J. D. Norley, R. Frayne, D. A. Steinman, and B. K. Rutt, "Characterization of common carotid artery blood-flow waveforms in normal human subjects," *Physiological Measurement* **20**, 219–240 (1999).
7. P. Kruizinga, F. Mastik, S. C. H. van den Oord, A. F. L. Schinkel, J. G. Bosch, N. de Jong, G. van Soest, and A. F. W. van der Steen, "High-definition imaging of carotid artery wall dynamics," *Ultrasound In Medicine and Biology* **40**, 2392–2403 (2014).
8. G. Dietsche, M. Ninck, C. Ortoft, J. Li, F. Jaillon, and T. Gisler, "Fiber-based multispeckle detection for time-resolved diffusing-wave spectroscopy: characterization and application to blood flow detection in deep tissue," *Applied Optics* **46**, 8506–8514 (2007).
9. T. Durduran, R. Choe, W. B. Baker, and A. G. Yodh, "Diffuse optics for tissue monitoring and tomography," *Reports On Progress In Physics* **73**, 076701 (2010).
10. R. C. Mesquita, T. Durduran, G. Yu, E. M. Buckley, M. N. Kim, C. Zhou, R. Choe, U. Sunar, and A. G. Yodh, "Direct measurement of tissue blood flow and metabolism with diffuse optics," *Philos Trans A Math Phys Eng Sci* **369**, 4390–4406 (2011).
11. T. Durduran and A. G. Yodh, "Diffuse correlation spectroscopy for non-invasive, micro-vascular cerebral blood flow measurement," *Neuroimage* **85 Pt 1**, 51–63 (2014).
12. D. A. Boas, S. Sakadzic, J. Selb, P. Farzam, M. A. Franceschini, and S. A. Carp, "Establishing the diffuse correlation spectroscopy signal relationship with blood flow," *Neurophotonics* **3**, 031412 (2016).
13. D. T. Wang, A. B. Parthasarathy, W. B. Baker, K. Gannon, V. Kavuri, T. Ko, S. Schenkel, Z. Li, Z. R. Li, M. T. Mullen, J. A. Detre, and A. G. Yodh, "Fast blood flow monitoring in deep tissues with real-time software correlators," *Biomedical Optics Express* **7**, 776–797 (2016).

14. D. A. Boas, "Diffuse photon probes of structural and dynamical properties of turbid media: Theory and biomedical applications," Ph.D. thesis, University of Pennsylvania (1996).
15. M. Belau, M. Ninck, G. Hering, L. Spinelli, D. Contini, A. Torricelli, and T. Gisler, "Noninvasive observation of skeletal muscle contraction using near-infrared time-resolved reflectance and diffusing-wave spectroscopy," *Journal of Biomedical Optics* **15**, 057007 (2010).
16. D. Bicoût and R. Maynard, "Diffusing wave spectroscopy in inhomogeneous flows," *Physica A* **199**, 387–411 (1993).
17. A. Zambanini, S. L. Cunningham, K. H. Parker, A. W. Khir, S. A. M. Thom, and A. D. Hughes, "Wave-energy patterns in carotid, brachial, and radial arteries: a noninvasive approach using wave-intensity analysis," *American Journal of Physiology-heart and Circulatory Physiology* **289**, H270–H276 (2005).
18. P. Reymond, F. Merenda, F. Perren, D. Rufenacht, and N. Stergiopoulos, "Validation of a one-dimensional model of the systemic arterial tree," *American Journal of Physiology-heart and Circulatory Physiology* **297**, H208–H222 (2009).
19. S. Sakadzic, D. A. Boas, and S. Carp, "Theoretical model of blood flow measurement by diffuse correlation spectroscopy," *Journal of Biomedical Optics* **22**, 027006 (2017).
20. E. J. Kroeker and E. H. Wood, "Comparison of simultaneously recorded central and peripheral arterial pressure pulses during rest, exercise and tilted position in man," *Circulation Research* **3**, 623–632 (1955).
21. G. Pucci, F. Battista, F. Anastasio, L. Sanesi, B. Gavish, M. Butlin, A. Avolio, and G. Schillaci, "Effects of gravity-induced upper-limb blood pressure changes on wave transmission and arterial radial waveform," *Journal of Hypertension* **34**, 1091–1098 (2016).

1. Introduction

Hypertension is a major risk factor for cardiovascular (CV) disease and thus to the development of many deaths by e.g. heart attack or stroke. In the current clinic practice only the systolic and diastolic blood pressure measured by brachial cuff sphygmomanometry is determined. Arterial stiffness which has an independent predictive value for cardiovascular events [1] and is suggested as a complement of systolic and diastolic pressure by brachial cuff sphygmomanometry [2] is usually not considered.

Elastic vessels have a low pulse wave velocity (PWV) and thus the reflected wave tends to return to the aortic root during diastole. In the case of stiff arteries the PWV rises and the reflected wave turns back earlier, adding to the forward wave and augmenting the systolic pressure [1]. This requires higher central pulse pressure and thus an increased systolic pressure which leads to an increased left ventricular load and a higher oxygen demand [1]. Arterial stiffness leads to an increased risk of stroke by remodeling of extra- and intracranial arteries due to an increased central pulse pressure and other mechanisms [1]. Arterial stiffness not only changes pulse wave velocity but also affects wave reflection. Therefore a direct measurement of the detailed temporal shape of the pulse is desirable.

The 'gold standard' for determining arterial stiffness is carotid-femoral PWV [1] which can simply be determined by measuring the pulse transit time at the two sites. This is often performed with arterial applanation tonometry, which however requires a mild pressure applied to the artery or photoplethysmography. Both modalities allow for the measurement of the pressure or distention curve, respectively, but do not allow for a measurement of the pulse blood flow profile. This might be achieved either by magnetic resonance imaging (MRI) [3–5] which requires a MRI facility and is expensive, or by ultrasound [6, 7]. For ultrasound measurements the detector has to be properly aligned and for a detailed analysis high frame rate ultrasound with high computational demand is required [7].

Here we present a proof of principle study of the application of a relative new optical measurement technique, Diffusing Wave Spectroscopy (DWS) also known as Diffuse Correlation Spectroscopy [8–12], which measures blood flow non-invasively. We show that this technique provides accurate temporal profiles of the blood flow pulse wave when a fast measurement system is used. In our case fast acquisition is realized by a hardware correlator with a temporal resolution of up to 6.5 ms as described in Dietsche et al. 2007 [8]. A similar temporal resolution has also been achieved recently using a software correlator [13]. The observed temporal profile of the blood flow pulse wave can be used to investigate e.g. wave reflections and to extract pulse wave velocity.

The optical measurement system is small and can be placed without the application of significant pressure. In addition, the placement, in particular the orientation of the measurement device is not as important resulting in robust signals. Proof of principle results for different arteries are shown as well as a continuous measurement at different blood pressures demonstrating the potential of the method not only for static but also for dynamic processes.

2. Methods

2.1. Diffusion wave spectroscopy

Diffusing wave spectroscopy measurements were performed with a fiber-multispeckle setup described earlier [8]. Light from a diode laser (TOPTICA, TA100) operating at $\lambda = 802\text{nm}$ is coupled into a multimode optical fiber to deliver light to the tissue surface. Multiple scattered light is detected at a distance $\rho = 20\text{ mm}$ from the injection point by a fiber bundle consisting of 32 single-mode fibers (Schäfter+Kirchhoff SMC-780) which probe statistically equivalent but independent speckles. In order to perform the experiments in the presence of ambient light a bandpass filter (Semrock FF01-800/12-25) centered at 800 nm is used in the receiver bundle. The light from each fiber is guided to an avalanche photodiode (APD; Perkin-Elmer SPCM-AQ4C). The output is connected to a custom build 32-channel multitaу hardware correlator (correlator.com) which continuously computes normalized autocorrelation functions $g_2(\tau)$ of the multiple scattered light intensity as a function of lag time τ with a integration time of 13 ms. The bundle-average intensity autocorrelation function is calculated by an intensity weighted sum $g_2(\tau, t) = \frac{1}{\sum_{i=1}^{32} C_i(t)} \sum_{i=1}^{32} C_i(t) g_{2_i}(\tau, t)$, where $C_i(t)$ and $g_{2_i}(\tau, t)$ is the average intensity and intensity autocorrelation function of the i -th fiber, respectively. The normalized intensity autocorrelation function is fitted by the solution of the correlation diffusion model for a semi-infinite geometry [14]:

$$g_2(\tau) = 1 + \beta \left| \frac{\exp[-\alpha(\tau)r_1] - \exp[-\alpha(\tau)r_2]}{\exp[-\alpha(0)r_1] - \exp[-\alpha(0)r_2]} \right|^2 \quad (1)$$

where $\alpha(\tau) = \left(3\mu_a\mu'_s + \mu'_s{}^2 k_0^2 \langle \Delta r^2(\tau) \rangle\right)^{1/2}$ is the dynamic absorption coefficient. The mean squared displacement is fitted both with a simple diffusion model ($\langle \Delta r^2(\tau) \rangle = 6D\tau$) and a mixed diffusion and shearing model ($\langle \Delta r^2(\tau) \rangle = 6D_{(2)}\tau + E_{(2)}\tau^2$) [15, 16]. The diffusion coefficient $D_{(2)}$ is proportional to blood flow [10–12] and $E_{(2)}$ accounts for any directed motion such as muscle movements [15]. The dominant term is given by the diffusion coefficient while the second gives an additional contribution during contraction and relaxation of the muscle. It turns out that the mixed diffusion-shearing model is a good way to reduce artifacts due to muscle motion. However, in the case of measurements on the common carotid artery there are additional contributions in the directed component which are not related to muscle motion, but might be due to tissue shearing (see discussion below).

The quantities $r_1 = (\rho^2 + z_0^2)^{1/2}$ and $r_2 = [\rho^2 + (z_0 + 2z_b)^2]^{1/2}$ are related to the depth $z_0 = 1/\mu'_s$ of the diffuse light source, the extrapolation length $z_b = 1/\mu'_s$ and the source detector separation ρ . The optical parameters have been fixed to the following values: absorption coefficient $\mu_a = 20\text{m}^{-1}$, reduced scattering coefficient $\mu'_s = 1200\text{m}^{-1}$, refractive index $n = 1.4$ and $k_0 = 2\pi n/\lambda$ denotes the wavevector. β is a coherence factor which accounts for the number of detected speckles and the detection optics and is about 0.5.

The assumption of fixed detection parameters μ_s and μ_a may lead to some systematic error in the determination of the absolute diffusion coefficient, but here, we are concerned only with relative changes. Dynamic changes in the effective absorption coefficient due to changes in blood volume during systole and diastole are relatively small (at most 10% change in count rate) and changes

in the effective scattering coefficient are expected to be small. Since the effective absorption coefficient (20 m^{-1}) is much smaller than the effective scattering coefficient (1200 m^{-1}) the optical path length distribution is hardly affected at all and therefore changes in the relative diffusion coefficient are almost only due to changes in the dynamics. We therefore think that it is not necessary to measure the optical parameters for the proposed applications.

2.2. Measurement protocol

Measurements were performed on a healthy 32 year old person (size: 1.72m, weight: 60kg, RR at measurement: 125/85).

The optical probe (Diffusing Wave Spectroscopy sensor) was consecutively placed at the distal end of A. radialis dextra in a sitting position (measurement at heart level) and standing position (measurement about 30 – 40 cm below heart level), on the A. carotis communis dextra (at height of Adam's apple - sitting position) and on A. dorsalis pedis dextra (standing position). At least three measurements of 60 s each were performed per site to verify reproducibility. In addition measurements on several days on the A. carotis and A. radialis showed a very good reproducibility. After each positional change a waiting time of several minutes was used to allow physiological parameters to reach a steady state. For optimal placement of the probe the artery is located by palpation and a very light pressure was used to press the probe onto the measurement site. Note that the waveform might be affected if stronger pressure is applied. Distances of the measurement sites from the 2. ICR at the sternum (measurement error up to ≈ 3 cm) to A. carotis, A. radialis (both standing and sitting) and A. dorsalis pedis are about 18 cm, 73 cm and 125 cm respectively.

In order to demonstrate the potential of the method for studying dynamic processes such as during a drug intervention affecting the blood pressure, a continuous measurement on the A. radialis dextra (sitting position) has been performed where the pressure in a brachial blood pressure cuff has been manually increased in steps of 10 mmHg every 20 s.

2.3. Electrocardiogram

An eeg (Delta 3 Plus, Cardioline) was recorded to synchronize the optical data with the electrical heart activity. The analog output (monitor output) of the eeg is sampled at 1kHz and digitized with an analog input module (NI PXI 4300). An artificial eeg produced by an arbitrary waveform generator (TGA 12101, TTI) which was both sampled electrically and by the eeg showed that the internal processing/filtering of the eeg produces a constant delay of 0.8625 s in the analog output. The eeg data has been corrected for this delay. Optical data and analog input data were further synchronized by a trigger which starts both measurements.

2.4. Data processing

First the positions of the R peaks in the eeg were detected by a custom written peak finder routine. The average heart rate period was calculated from the peak positions. Then the data (both eeg and DWS) of every heart beat were interpolated to the length of the average heart cycle. Finally, the average waveform was determined by averaging all interpolated heart cycles within the measurement time (60 s).

Note that all features of the blood pulse profile can already be seen without averaging (Fig. 1). Due to the sampling with 13 ms the raw DWS data are not as smooth as the averaged data while they allow for the observation of fast dynamic changes. The relative change of the diffusion coefficient has been calculated by first normalizing the diffusion coefficient by dividing the average over the measurement period and then subtracting 1.

The peak positions of the DWS data were determined following the nomenclature of [4, 5]: First the maximum of the averaged pulse wave was found. The exact peak position of P1 was determined by a peak finder routine (FindPeak, WaveMetrics IgorPro) which searches for

the peak in the range ± 13 ms of the location of the maximum. The points M0 and M1 were determined by finding the first minimum before and after P1, respectively. The peak P2 was determined by the first positive peak after M1, M2 as the first minimum after P2 and so on. If only two instead of three peaks are observed the values of M1 and P2 are assigned to M2 and P3.

3. Results

Figure 1 shows exemplary data of the unaveraged normalized diffusion coefficient (rel D). A sharp increase which peaks about 0.127 s after the R peak of the ecg followed by a steep decrease with a second smaller peak centered at around 0.303 s (average heart rate 82.3 bpm) is observed. The changes are clearly visible in the unaveraged data and therefore can be used to track dynamic changes in the blood flow waveform.

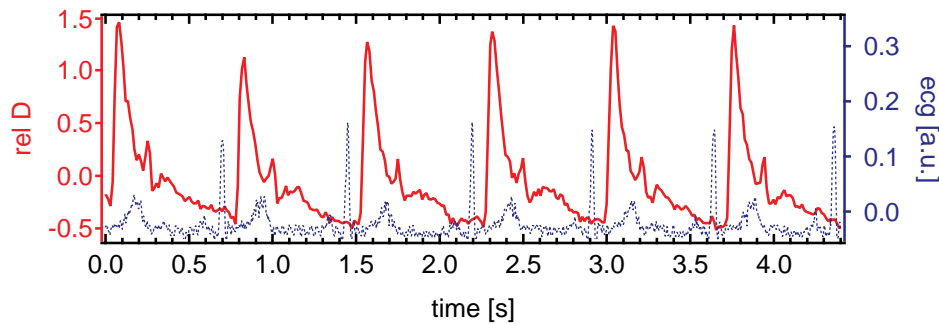


Fig. 1. Relative diffusion coefficient (rel D - red solid lines) and ecg (blue - dotted line) of the measurement on the A. carotis communis dextra.

In order to analyze the features of the blood flow waveform in more detail, the individual waveforms of one heart beat were averaged during a period of 60 s, which, depending on heart rate, corresponds to an average over 82 to 92 individual waveforms (see section 2.4 for details). Fig. 2 shows the averaged waveform for the common carotid artery, the radial artery and dorsalis pedis artery. For the carotid artery the average shape of the diffusion coefficient in the diffusion only model (solid lines) and mixed diffusion shearing model (dashed lines) differs in that the first peak (P1) is delayed in the second case and there is only a shoulder compared to a second peak (P2) in the diffusion model. This is followed by a more shallow third peak (P3). The differences in the two fit models result from additional contributions of a directed movement. The waveform of the directed movement shows three peaks located at 97ms, 205ms, 306ms and relative heights of 4.79, 0.47, 1.05, respectively.

For the radial and dorsalis pedis artery the waveform is the same for both the diffusion and mixed diffusion-shearing model. One also finds three peaks in the radial artery if the patient is standing but only two peaks in the sitting case where the second peak can be seen as shoulder. A similar behavior is found for the dorsalis pedis artery.

The broadening of the peaks due to wave dispersion with traveled distance can also be seen. Peak positions of the waveform from the different arteries are summarized in table 1. One finds that the peak positions of M0, P1, M2 and P3 are observed at later times in the order A. carotis < A. radialis (standing) < A. radialis (sitting) < A. dorsalis pedis while M1 and P2 (or the shoulder) is observed at about the same time. For the peaks that change their position the relative distance is relatively constant with a delay of -86 ± 15 ms, 186 ± 23 ms and 258 ± 15 ms for M0 minus P1, M2 minus P1 and P3 minus P1, respectively.

Figure 3 shows a continuous measurement on A. radialis dextra (sitting position) where the brachial cuff pressure has been increased by 10mmHg every 20s. The curves show the average

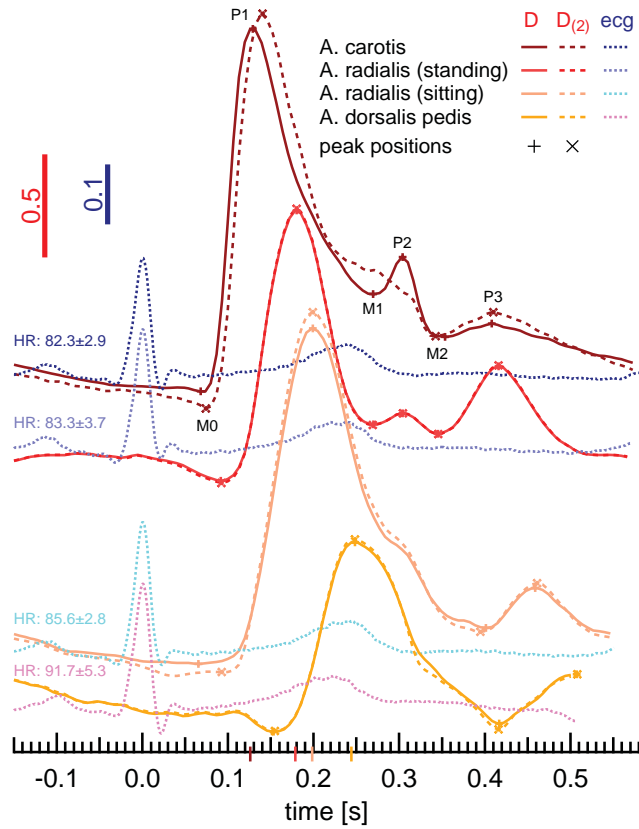


Fig. 2. Average waveform of the diffusing wave spectroscopy data fitted with the diffusion model (D - solid lines) and the mixed diffusion-shearing model ($D_{(2)}$ - dashed line). The average ecg of the measurements is shown as dotted lines. Red scale bar indicate the relative amplitude of the change after normalization of the optical data to the average value during measurement. Blue scale bar is the amplitude of the ecg in arbitrary units. Measurements are from top to bottom: A. carotis communis dextra (sitting position), A. radialis dextra (sitting position), A. radialis dextra (standing position) and A. dorsalis pedis dextra (standing position). Peak positions of D are additionally marked as a guide to the eye on the timeline.

Table 1. Average time in ms from R peak of ecg till peaks in the diffusion coefficient. Peaks are determined as described in the text. *peak was incorrectly determined as 66ms by the peak finder procedure, due to no clear minimum. Used bottom-up segmentation of waveform to determine peak onset instead of procedure described above.

	location	M0	P1	M1	P2	M2	P3
D	A. carotis	68	129	269	304	353	408
	A. radialis (standing)	92	180	270	304	345	416
	A. radialis (sitting)	106*	199	-	-	401	459
	A. dorsalis pedis	153	248	-	-	417	507
$D_{(2)}$	A. carotis	74	140	-	-	343	410
	A. radialis (standing)	92	180	269	304	346	416
	A. radialis (sitting)	93	199	-	-	395	461
	A. dorsalis pedis	155	248	-	-	416	508

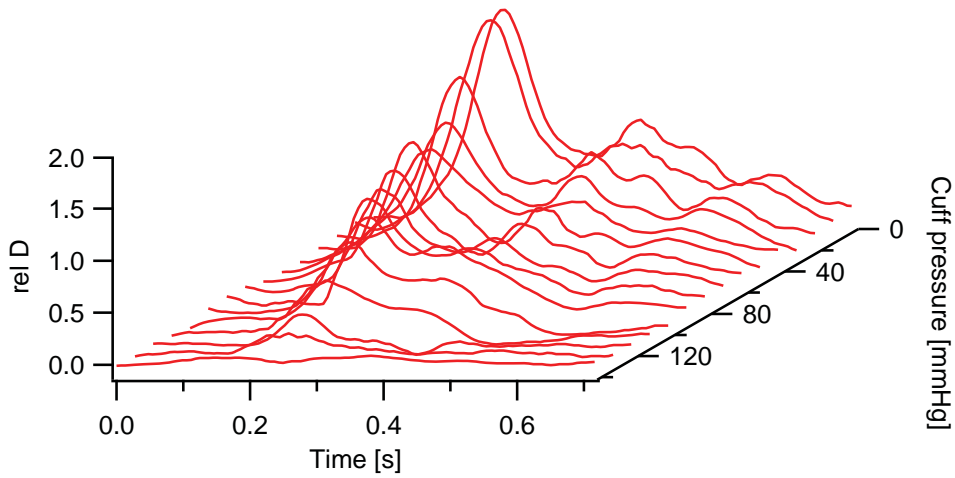


Fig. 3. Changes during occlusion of the brachial artery while measuring at the radial artery. The cuff pressure has been manually increased by 10mmHg every 20s (from back to front). Each curve represents the average waveform of 10s. It can be nicely seen that a shoulder instead of a second peak develops when the cuff pressure reaches the diastolic blood pressure.

blood flow waveform of 10 s. One finds a steady decrease of P1 with increasing pressure until the flow ceases at 140 mmHg. The second peak is also reduced with increasing pressure and passes in a shoulder when the cuff pressure reaches diastolic pressure.

4. Discussion

The measured temporal blood flow profile of the carotid artery is in good agreement with previous measurements [17, 18]. It has to be noted that the mixed diffusion-shearing model, with both a diffusive and directed contribution in the mean squared displacement (MSD), better resembles the published results. One explanation for such a behavior is shearing of the surrounding tissue due to distention of the artery leading to additional contributions. The same effect is observed during muscle contraction [15] and can be used to reduce motion artifacts. Another explanation might be that the MSD $\langle \Delta r^2(\tau) \rangle = 6D_{(2)}\tau + v_{RBC}^2\tau^2$ of the blood flow has both diffusive and directed contributions [12]. While the directed contributions can usually be neglected in small vessels, they might have to be considered for large vessels with a high blood flow velocity [19]. A definitive assignment to one of the two explanations could not be made but the use of the mixed-shearing model will account for this effect regardless of its physical origin. In the case of no directed motion in the MSD the two models give the same result but the diffusion only fit is more robust.

The waveforms of the radial and dorsalis pedis artery are similar to the pressure waveforms reported by Kroecker et al. [20]. Furthermore, it was demonstrated that the measured blood flow profile is affected by the position of the patient (sitting, standing) and deviations also occur in the waveform dependent on the angle of the arm (data not shown). This is in agreement with measurements of Pucci et al. [21] who recently reported similar observations. The same effect is observed if a strong pressure is applied to the artery (mild pressure has only negligible effects). The big advantage of DWS is that the probe orientation is not important for the measurement and robust and reproducible results are obtained on the same subject if the subjects position is the same. For a comparative study with different patients, or consecutive measurements in one patient, it is thus of utmost importance that all patients be positioned the same way.

Dynamic changes in blood flow profile during increasing brachial cuff pressure have also been studied. The blood flow curves are not as smooth as in the former case because the pressure was manually increased by the subject itself leading to some motion artifacts. However, this demonstrates the robustness of the method also in agitated patients. Dynamic changes are particularly interesting to directly monitor changes in the blood flow profile during interventions such as during drug induced blood pressure management. One has to note that the measured signal is only proportional to blood flow and absolute blood flow values can only be determined by proper calibration, since the proportionality factor is affected by the vessel size and the hematocrit [12, 19]. However, if these two parameters are known approximate conversion factors might be determined [12, 19] and used in future studies. For PWV measurement and waveform analysis the relative values are sufficient.

5. Conclusion

Diffusing Wave Spectroscopy was introduced in a proof of principle study in one subject as a new, non-invasive and portable tool for pulse blood flow waveform analysis. It might also be used for pulse wave velocity measurements by measuring either at two sites simultaneously or with ecg synchronization. Furthermore it enables a continuous measurement of the blood flow profile during interventions which allow for the direct control of the effect and might help in guiding decision making in the therapy of hypertension.

Funding

Deutsche Forschungsgesellschaft (DFG),(MA 817/9-1).